Research Square

Preprints are preliminary reports that have not undergone peer review.
They should not be considered conclusive, used to inform clinical practice,
or referenced by the media as validated information.

Experimental research on damage evolution and stability control of surrounding rock in deep coal mines

Chongyan Liu
Anhui University of Science and Technology
Longpei Ma
nongfu320@163.com

Anhui University of Science and Technology
Guangming Zhao
Anhui University of Science and Technology
Qihang Zhang
Anhui University of Science and Technology
Cheng Pan
Anhui University of Science and Technology

Research Article

Keywords:

Posted Date: November 13th, 2026

DOI: https://doi.org/10.21203/rs.3.rs-11347090/v1

License: This work is licensed under a Creative Commons Attribution 4.0 International License.
Read Full License

Additional Declarations: No competing interests reported.

Experimental research on damage evolution and stability control of surrounding rock in deep coal mines

Chongyan Liu[a, b], Longpei Ma[b, c*], Guangming Zhao[a, c], Qihang Zhang[b], Cheng Pan[d]

[a] *Key Laboratory of Safe and Effective Coal Mining, Ministry of Education of China, Anhui University of Science and Technology, Huainan 232001, China*

[b] *Joint National-Local Engineering Research Centre for Safe and Precise Coal Mining, Anhui University of Science and Technology, Huainan 232001, China*

[c] *School of Mining Engineering, Anhui University of Science and Technology, Huainan 232001, China*

[d] *School of Civil Engineering and Architecture, Anhui University of Science and Technology, Huainan 232001, China*

*** Corresponding author: Longpei Ma**

Corresponding address: Anhui University of Science and Technology, Huainan, Anhui 232001, China

E-mail: nongfu320@163.com

Tel: +86 17309646702

Article highlights

- A three-tier strategy integrates support, grouting, and borehole pressure relief.
- Physical models reveal damage evolution and stress transfer during unloading.
- Unsupported rock damage drives peak stress migration into deeper regions.
- Hierarchical control maintains support stability at twice the in-situ stress.
- Field monitoring confirms reduced roadway deformation and improved stress states.

Abstract This study proposes a hierarchical control concept and establishes a three-tier support system to address the control challenge of severe stress concentration and damage in roadway surrounding rock mass induced by stress redistribution during deep coal mining. A combined approach of similar-material physical modelling and digital-image techniques is employed to elucidate the stress-transfer mechanism and damage evolution of the surrounding rock mass during unloading under different support conditions, and the findings are validated through field engineering tests. Results show that, in the absence of support, increasing confining pressure drives crack propagation to greater depths of the surrounding rock mass; the lateral abutment pressure first increases and then decreases, and the stress peak migrates toward the deeper rock mass. With the hierarchical control technology, the synergistic load-bearing performance of the support system is markedly improved; deformation of the surrounding rock mass becomes more uniform; stresses within the anchorage system increase in a stable manner; and no support failure is observed. Field application confirms the effectiveness of the hierarchical control strategy: the surrounding-rock stress state is substantially improved and deformation is restrained, providing a reliable technical pathway for stability control of deep roadways.

Keywords Deep coal mine roadways · Excavation unloading · Damage evolution · Hierarchical control · Physical modelling ·

1 Introduction

Deep surrounding rocks possess a high-stress attribute due to the superposition of the original and tectonic stress fields (Yang et al. 2017; Zhu et al. 2017). The excavation of roadways induces alterations in the stress state of the surrounding rock mass, causing stresses to progressively redistribute toward a novel equilibrium state. During this adjustment process, the free space generated by unloading can lead to reduced radial stress in the unloading region and increased tangential stress concentration. The influence of nearby disturbances exacerbates stress concentration, which may cause damage and cracking in the surrounding rock. This may lead to rock splitting, rock spalling, and a weakening or failure of the support system, which can result in hazards such as roof falls and rock bursts (Si et al. 2024; Qiu et al. 2025; Cai et al. 2017; Wang et al. 2024).

Currently, the majority of research focuses on the control of roadway deformation (Bednarek et al. 2024). The common fundamental support methods include hydraulic supports, anchor rods, anchor cables, and metal mesh. The team led by Academician Hongpu Kang suggests that surrounding rock control after roadway excavation should focus on both internal support and reinforcement measures. They have effectively controlled catastrophic rock deformation using a combined support that integrates anchor-mesh-cable-shotcrete, hydraulic supports, and grouting (Li et al. 2025; Kang et al. 2023). Li et al. (2016) conducted a systematic investigation of the influence exerted by key mechanical properties in surrounding rock formations on interfacial bonding characteristics. Furthermore, the researchers designed and optimized an innovative grouted anchor

system, which has been validated through field implementations. Zhao et al. (2020) conducted a comprehensive analysis of stress distribution characteristics and key controlling parameters in fully-grouted anchor systems during progressive rock mass deformation. Xie et al. (2022) investigated the damage characteristics of surrounding rock in deep coal roadways subjected to dynamic pressures and identified challenges in controlling surrounding rock deformation. In addition, they proposed a synergistic control technique that integrates external anchoring with internal unloading to address significant roadway deformations. Chen et al. (2020) revealed the composite damage mechanisms of surrounding rock in coal roadways based on stress differences between deep and shallow anchor cables. Furthermore, they suggested a control technique that combines anchoring and unloading. Malkowski et al. (2019) found that fracturing decreases a rock mass quality what in turn change rock mass parameters and affects the range of damage zone around mining working. Zhuang et al. (2023) used numerical methods to demonstrate that the effects of mining earthquakes on a roadway can be reduced by constructing an artificial weakening zone. Kang et al. (2017) elucidated the softening characteristics of the roadway roof and coal body. Subsequently, they proposed truss anchoring cable control technology. Xiang et al. (2021) and Xie et al. (2023) focused on the issues associated with interbedded coal and rock roadways to reveal the mechanisms underlying uneven deformation in surrounding rock. They proposed an enclosed support method centered on active support measures, including anchor rods, anchor cables, and grouting, to effectively control deformation in gob-side entry retaining. Extensive research exists on methods for stabilizing surrounding rock; however, these methods primarily rely on the anchor rods, metal mesh, and anchor cables, while other control measures serve as supplementary support techniques.

Regarding the similar model experiments for deformation and damage of surrounding rocks in

84 roadways, A. N. Romashov et al. (1993) were the first to establish a conceptual physical model in
85 1993 for simulating the failure of layered rock masses. Dong et al. (2018) designed an experimental
86 system that accounts for the initial geo-stress and dynamic unloading to investigate the unloading
87 effects in the surrounding rock during cyclic dynamic excavation. Wu et al. (2022) conducted a
88 systematic review of key methodological approaches in rock burst analysis, encompassing
89 theoretical frameworks, numerical simulations, laboratory-scale physical modeling, and in-situ
90 monitoring systems. Nan (2012) revealed the stress evolution process of jointed and fractured rock
91 roadways from excavation unloading to deformation and failure by combining physical similarity
92 simulation with numerical calculation. The study indicated that instability modes such as roadway
93 collapse, rock burst, and floor heave are mainly controlled by the rock mass structure, while the
94 deformation intensity is closely related to the in-situ stress level. Peng et al. (2023) conducted true
95 triaxial tests on granite specimens with controlled arch geometries to replicate the spalling process
96 under diverse in-situ stress regimes. The investigation elucidated stress distribution patterns and
97 spalling mechanisms within peripheral rock mass of deep underground excavations. Zhang et al.
98 (2024) employed circular boreholes and artificially induced fractures to replicate geological
99 discontinuities. Comparative analyses were conducted on fracture progression, acoustic emission
100 signatures, and failure modes between intact and discontinuum specimens under controlled loading
101 conditions. J. Vacek et al. (2008) demonstrated the failure of the hole model through physical
102 experiments and employed mathematical models to elucidate the mechanisms behind surrounding
103 rock failure in coal mine roadways. Sun et al. (2024) categorized the failure of soft rock roadways
104 into four stages through a combination of model experiments and numerical simulations.
105 Nevertheless, there are numerous factors that contribute to the deterioration and instability of

surrounding rock. and relying solely on primary support is inadequate for maintaining their long-term stability. Therefore, it is essential to consider the specific challenges and engineering conditions to propose effective strategies for stabilizing unloaded surrounding rock. This will further enhance the control system for surrounding rock.

This study proposed a grading control strategy to address the challenges of managing deformation in the unloaded surrounding rock through a comprehensive analysis of on-site failure causes. This strategy includes primary support for crack prevention, reinforced anchor grouting for crack reduction, and localized drilling for pressure relief. Additionally, comparative similar model experiments were conducted to comparatively analyze the damage evolution in supported and unsupported surrounding rocks, thereby clarifying the effectiveness of the grading control strategy in managing unloaded surrounding rock. The implementation of this strategy in engineering practice has demonstrated significant reduction in deformation of surrounding rock strata. These findings offer critical theoretical guidance for the design of surrounding rock support systems in analogous geotechnical environments.

2 Engineering geology

The 1302 longwall mining face at Shaanxi Zhaoxian Coal Mine is situated at vertical depths ranging from 540 m to 640 m, characterized by an average seam thickness of 9.1 m, strike azimuth of 170°-240°, and an average dip angle of 15°. The panel dimensions comprise a strike length of 1,650 m along the coal seam axis and an inclination span of 163 m perpendicular to the strike direction. Geological modeling indicates estimated recoverable reserves of 3.2991 million metric tons within the delineated block. The spatial configuration of the mining face relative to geological structures is schematically represented in Fig. 1.



Fig. 1 Failure of the surrounding rock

As depicted in Figure 1, significant deformation, localized roof sinking, and failures of anchor rods and anchor cables occurred at the 1302 working face after roadway excavation and unloading, which pose significant safety risks to the mining operations.

3 Analysis of causes of roadway damage and grading control strategy

3.1 Analysis of causes of surrounding rock damage in the roadway

(1) Poor surrounding rock conditions. The 1302 work face is fragmented, with the coal primarily manifesting in both block and debirs forms. The immediate roof and floor regions demonstrates unfavorable conditions due to a high degree of initial damage, which is characterized by significant joint development and numerous cracks.

(2) Intense excavation unloading effect. The rapid excavation rate at the 1302 work face significantly affects the surrounding rock. The excavation unloading effect causes rapid crack propagation that fosters the development and connection of shallow cracks and accelerates

nonlinear deformation damage.

(3) Noticeable stress concentration in the surrounding rock. Field monitoring data indicated that local stress in the 1302 work face reached twice the theoretically calculated geo-stress. This has caused the cracks in the surrounding rock to extend into deeper regions. Moreover, the substantial accumulation of elastic energy in the surrounding rock increases the risk of various failures, including rock spalling, rock bursts, and coal bursts.

3.2 Grading control approach

A comprehensive grading control approach, which integrates primary support for crack prevention, reinforced anchor grouting for fracture mitigation, and targeted borehole drilling for stress redistribution, was proposed to mitigate deformation control challenges in surrounding rock formations, as detailed in Fig. 2.

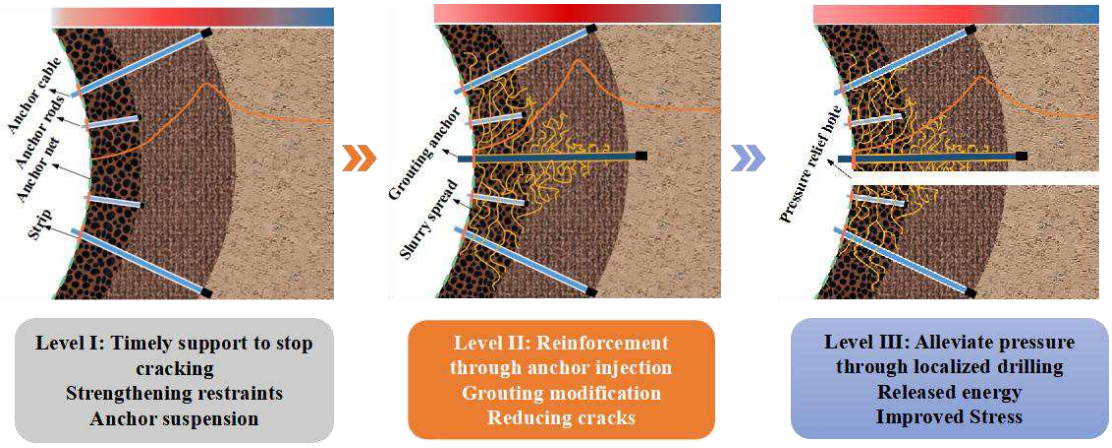


Fig. 2 Surrounding rock failure and control methods

Level I control focuses on the primary support to prevent cracks. Support measures including anchor rods, metal mesh, anchor cables, and steel beams should be promptly implemented to preserve the structural integrity of the surface layer in surrounding rock. High-prestressed anchor rods and diamond-shaped metal mesh can be utilized to establish a preliminary shallow load-bearing structure to prevent rapid expansion in the residual zone. Additionally, the implementation of anchor

cables, steel strips, and steel beams effectively enhances the prestress diffusion in the anchor rod support system. This approach not only restores the radial stress in the anchorage region but also enhances the ultimate load-bearing capacity. Furthermore, it effectively mitigates both discontinuous and uncontrolled deformation in the unloaded surrounding rock.

Level II ground control measures comprise systematic reinforced anchor grouting as a primary stabilization mechanism for fracture mitigation. As mining progresses, noticeable stress concentration occurs due to mining impacts and disturbances. Progressive crack development within excavation-damaged zones induces progressive deterioration of key geotechnical parameters including shear strength, tensile strength, cohesion, and friction resistance. Consequently, the tensile and shear stress on the anchor rods increases, which make them prone to anchor pull-out and breakage. To address this issue, reinforced support measures are undertaken to reduce cracks. This is achieved by employing grouted anchor cables while simultaneously installing grouting devices to achieve integrated anchoring and grouting. The grouting fills and consolidates pores and cracks. The diffusion of the grout in shallow regions forms a grouted body, which enhances the load-bearing capacity. The grout in deep regions mitigates discontinuous deformation, such as delamination and crack propagation in the plastic zone. This significantly improves the load-bearing capacity of the degraded unloaded surrounding rock and ensures the long-term stability of the anchorage load-bearing structure.

Level III control relies on localized drilling to relieve pressure. Pressure relief through drilling is an effective approach to modify the stress state in the surrounding rock for ensuring its stability. Although primary Level I and secondary Level II containment strategies demonstrate efficacy in mitigating deformations, substantial residual strain energy persists within the rock mass at critical

threshold levels. This necessitates the implementation of Level III control measures. Pressure-relief boreholes employ strategically configured borehole cavities to facilitate controlled dissipation of volumetric-expansion-induced deformations, thereby enabling optimized management of strain energy release in geotechnically constrained deep roadway environments. This approach not only redistributes the highly concentrated stress around the coal roadway but also releases some energy. This reduces the potential damage caused by concentrated stress to the support structure and ensures the stability of the shallow surrounding rock.

4 Analysis of damage evolution in unloaded surrounding rock under grading control

4.1 Experimental design

Similar simulation experiments were conducted to determine the effectiveness of grading controls. The model tests were performed using an anchorage bearing mechanical simulation system for surrounding rock, as illustrated in Figure 3. The similarity ratios for geometry, specific weight, stress, and time were 1:20, 1:1.5, 1:30, and 1:4.47, respectively. The similar materials were prepared using river sand, calcium carbonate, lime, gypsum, and water in a mass ratio of 96.2:3.15:4.61:4.82:11.8.

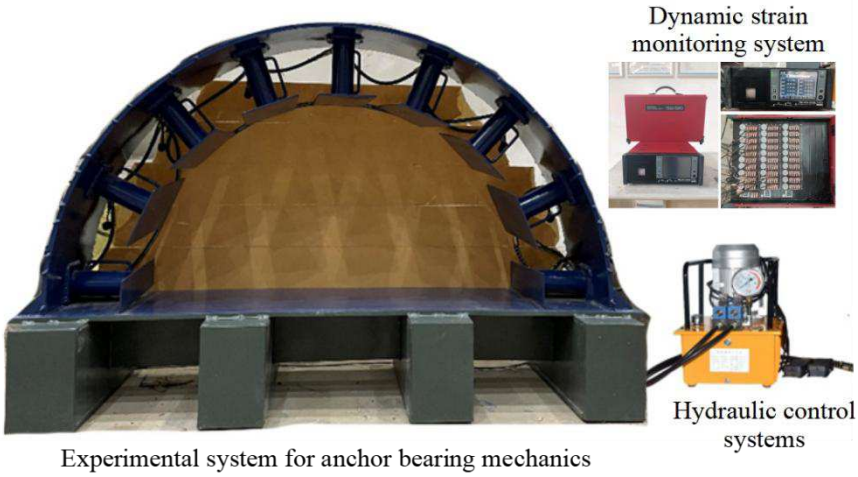
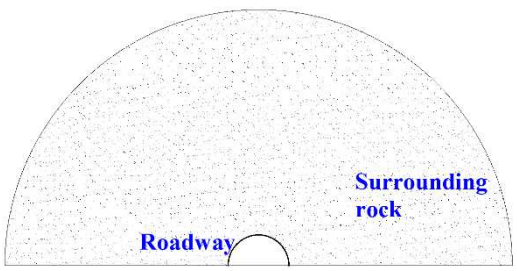


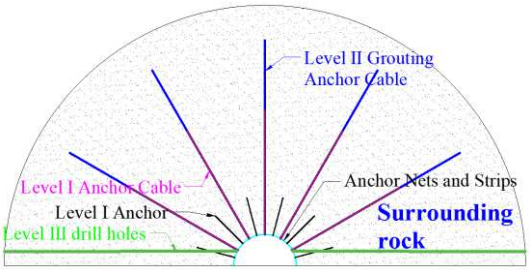
Fig. 3 Test system for anchorage bearing capacity simulation of surrounding rocks

The simulation approach of pre-buried equivalent layer was used to simulate gradually, and the thickness of the equivalent layer was determined based on the larger fractured area of the surrounding rock in the unsupported condition (Liu et al. 2025a). The grout analog materials consisted of river sand, calcium carbonate, lime, gypsum, cement, and water in a mass ratio of 96.2: 3.15: 4.61: 4.82: 3.32: 11.8. The optimized composite exhibited a uniaxial compressive strength of 0.7 MPa, representing a 1.52-fold increase compared to conventional surrounding rock analogs.

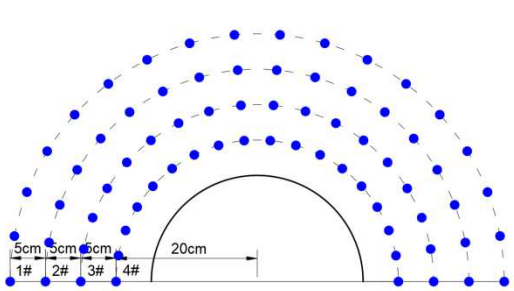
Based on the surrounding rock conditions at the construction site, equivalent circular radii were calculated and utilized in the experiment design, and the roadway radius was designed to be 30cm. Fig. 4 presents the physical similar model experiment scheme. The testing process consisted of three stages: initial geo-stress loading, roadway excavation and support, and graded step loading. A stepwise loading approach was used to simulate stress concentration, and each level of stress was maintained for three hours. Data monitoring was performed using a static strain testing analysis system and a camera system.



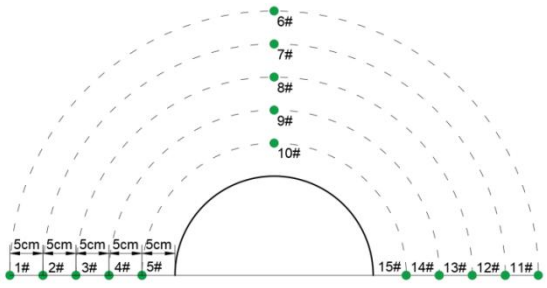
(a) Uncontrolled



(b) Grade control



(c) Displacement measuring point



(d) Stress measurement point

Fig. 4 Test programme for anchorage similarity simulation

4.2 Similar materials for anchor rods and anchor cables

In the model tests, four prototype anchor rods were equivalent to one model anchor rod, while two prototype anchor cables were equivalent to one model anchor cable (Yang et al. 2019; Liu et al. 2019; Wang et al. 2019). Anchor rods were fabricated from 1.1-mm-diameter tin wire with 120 mm length. Grade I and II anchor cables were constructed using 1.1 mm diameter aluminum wire with lengths of 310 mm and 430 mm, respectively. Anchor rod plates were fabricated from 0.5-mm-thick iron sheets with 7.5 mm square dimensions, whereas anchor cable plates employed 0.75 mm thick sheets of 15-mm square size. A metal mesh with an 8-strand configuration was used, and the steel strips were simulated using 9 mm wide and 0.25 mm thick aluminum tape.

The prototype pressure relief borehole features a 153 mm diameter, therefore the model boreholes were scaled to 8 mm diameter with 500 mm depth. Four boreholes were arranged laterally with 100 mm spacing. Key improvements: Model anchor rods and anchor cables were embedded in the grading control model, and pre-tension was applied after roadway excavation to simulate support. Subsequently, model plates, metal mesh, and steel strips were installed and tightened with M2 nuts to exert pre-tension on the anchor rods and anchor cables after roadway excavation.

The key steps in model preparation include material ratio formulation, model assembly, sensor installation, model curing, sealing, and monitoring, as illustrated in Fig. 5. A stress protocol corresponding to in-situ stress conditions, was employed for loading to elucidate the damage evolution of the surrounding rock (Liu et al. 2025b), as illustrated in Table 1.



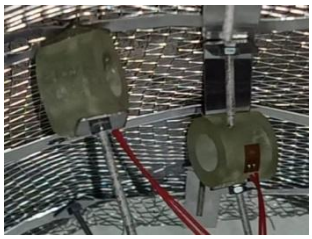
(a) Model preparation



(b) Roadway excavation



(c) Installation of anchor cables



(e) Strain gauge for anchor rods and cables



(f) Drilling



(g) Experimental model

Fig. 5 Simulation of the experimental process

Table 1: Graded loading stress nodes of the surrounding rock

Number of load cycles	Experimental scenario	Interval time /h	Internal load /MPa
1	600m	3	16.20
2	Roadway excavation	3	16.20
3	600m*1.2 (Mining-induced impact)	3	19.44
4	600m*1.4 (Mining-induced impact)	3	22.68
4	600m*1.6 (Mining-induced impact)	3	25.92
5	600m*1.8 (Mining-induced impact)	3	29.16
6	600m*2.0 (Mining-induced impact)	3	32.40

5 Results and analysis

5.1 Experimental design

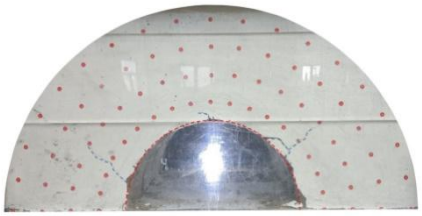
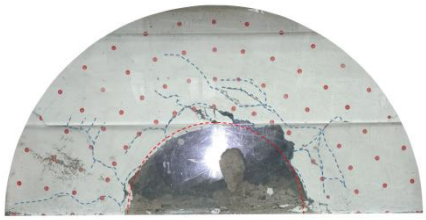
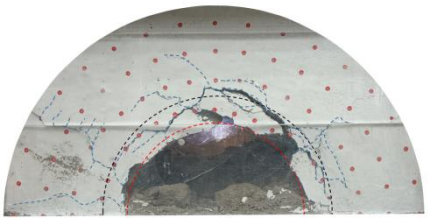
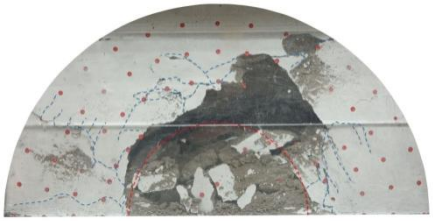
5.1.1 Deformation and damage characteristics

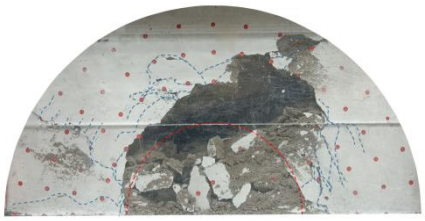
The full-sequence deformation behavior of excavated high-stress surrounding rock formations was monitored through the XTDIC-CONST non-contact 3D optical strain displacement measurement

240 system. The temporal characteristics of crack development initiation,propagation,andcoalescence

241 within the cross-section are quantitatively documented in Table 2.

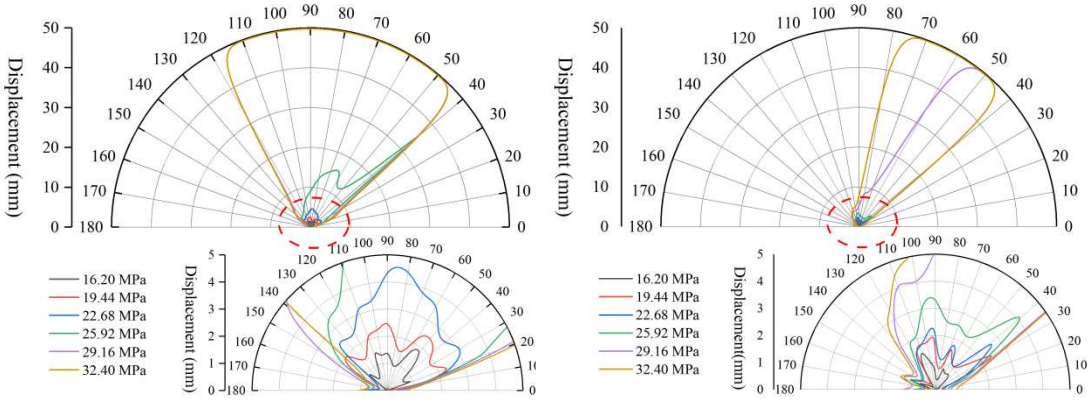
242 Table 2: Deformation and failure characteristics in roadway sections

Internal load /MPa	Cross-section diagram	Deformation characteristics
16.20		At a depth of 600 m, cracks initially emerged in the roadway cross-section and then extended from the roadway surface into the deeper surrounding rock. Additionally, cracks appeared on the internal roadway surface, accompanied by falling debris.
19.44		Cracks on the right side of the roadway expanded extensively, while detachment of fragments occurred near the roadway surface, and the number of falling debris within the roadway increased.
22.68		Cracks in the cross-section extend deeper in a circular pattern. Partial collapse of the surrounding rock occurred in some regions.
25.92		Cracks continued to develop and expand. The trend of interconnected cracks in the shallow regions was more pronounced than that in the deeper regions. The surrounding rock underwent significant deformation. A considerable number of debris accumulated in the roadway, and the fractured zones exhibited an arc-like feature. These observations indicated that the surrounding rock had largely lost its load-bearing capacity.
29.16		The surrounding rock in the fractured zones completely collapsed, leading to the significant development of deep cracks. The roadway lost its load-bearing capacity, and its interior was filled with debris from the surrounding rock, resulting in a loss of its original shape.

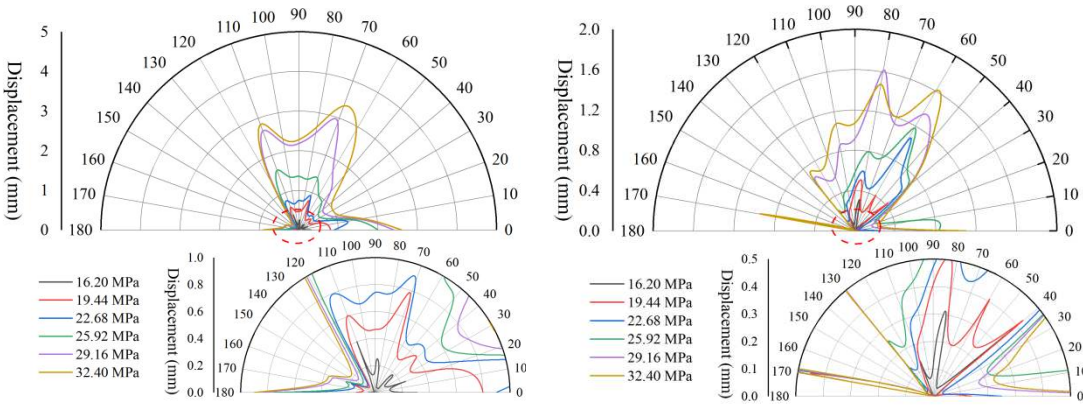
32.40		The collapsed and fragmented area expanded significantly, with large fragments falling and accumulating. The external loads led to the ongoing development and penetration of cracks in the surrounding rock.

Displacements at various measurement points relative to the roadway center were recorded under different stress concentration conditions, as shown in Fig. 6.

Analysis of displacements at varying depths revealed that rock failure primarily concentrated within a range of 10 cm form the roadway's contour. As the distance from the roadway's contour increased, both the significant deformation area and failure area diminished. Within a 10 cm radial distance from the roadway's contour, the surrounding rock mass exhibited quasi-homogeneous deformation characteristics under applied stress levels not exceeding the 25.92 MPa threshold. As high stress became concentrated, deformations in both shallow and deep regions gradually intensified. When the external load exceeded 25.92 MPa, the roadway underwent significant deformation, and the surrounding rock displayed cracking and instability. It was evident that instability occurred in the deep surrounding rock under a scenario of 1.6 times the stress concentration. The main area of large deformation instability was located within 10 cm form the roadway's contour.



(a) 20 cm from the center of the roadway (b) 25 cm from the center of the roadway



(c) 30 cm from the center of the roadway (d) 35 cm from the center of the roadway

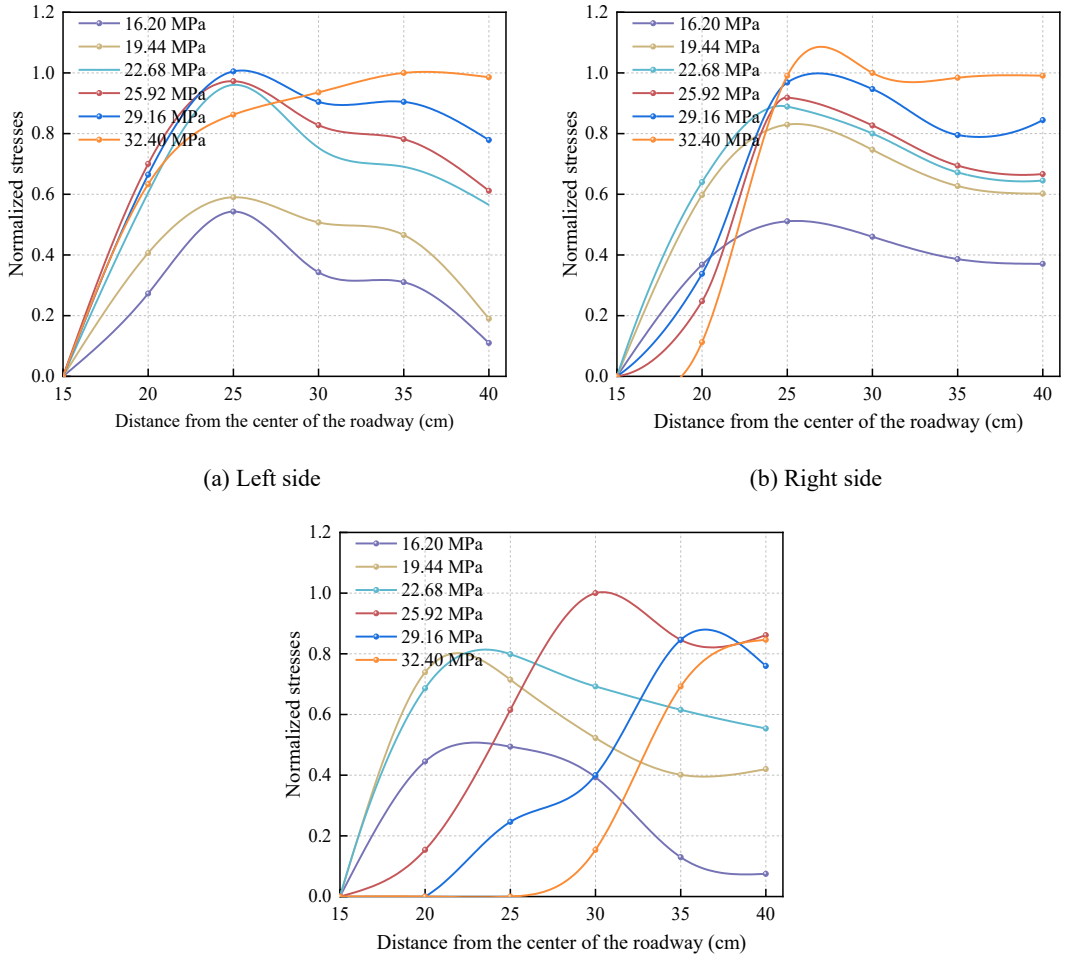
Fig. 6 Macroscopic and detailed results of displacement variation at different depths of the surrounding rock

5.1.2 Evolution characteristics of surrounding rock stress

The stress data obtained from the pressure cells was normalized and is presented in Fig. 7. When the external load reached 16.20 MPa, the surrounding rock stress exhibited an initial increase followed by a subsequent decrease as the distance from the roadway wall increased. Maximum stress concentration was observed at a radial distance of 5-10 cm form the roadway's contour. The surrounding rock stress peaked at 10 cm from the roadway's contour before exhibiting a gradual decline. When the external load increased to 22.68 MPa, fracturing zone began to develop in the shallow surrounding rock, and cracks started to propagate and penetrate (see Fig. 7(c)). Concurrently, the stress at a point 5 cm from the roadway's contour showed a slight decrease. This indicated the onset of damage and fracturing in the shallow surrounding rock and a reduction in its load-bearing capacity.

At an external load of 25.92 MPa, significant damage was observed in the shallow surrounding rock on the right side (roadway top). The stresses at positions 5 cm and 10 cm from the roadway's contour showed a decline. Meanwhile, the peak load in the deep surrounding rock increased, as it shifted from shallow to deeper regions. As the external load continued to increase, substantial fragmentation of the surrounding rock occurred. The stress exhibited a decrease in shallow regions

and an increase in deep regions, and the peak stress shifted to deeper regions.



(a) Left side

(b) Right side

(c) Top

Fig. 7 Stress distribution characteristics at different locations in the unloading surrounding rock

5.2 Damage evolution under grading control

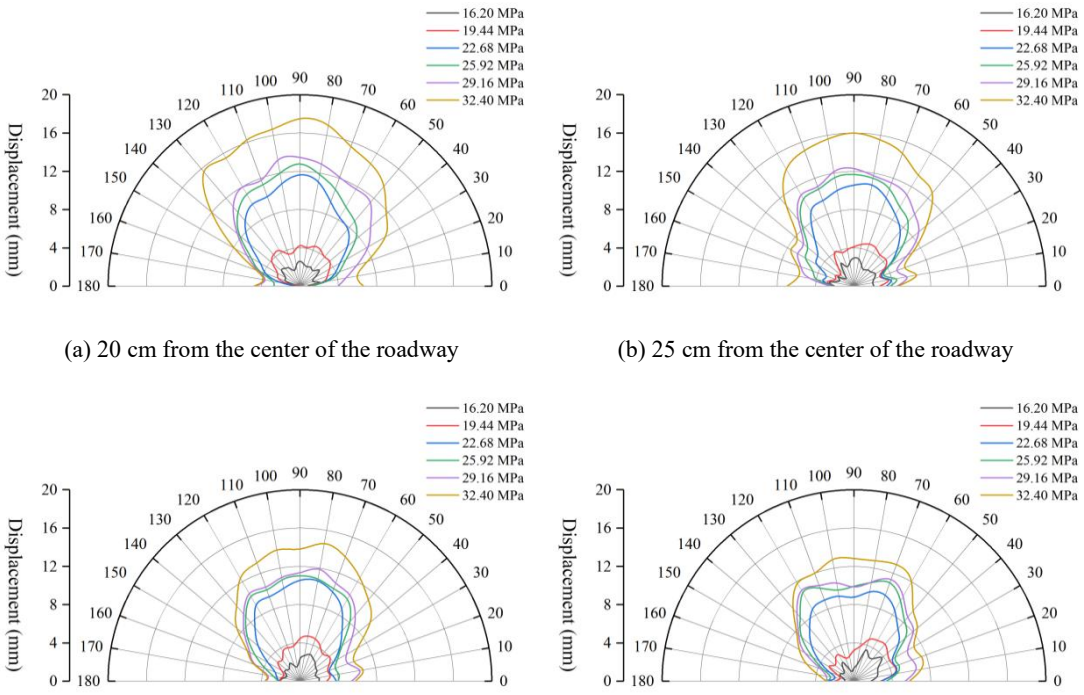
5.2.1 Deformation and damage characteristics

When the external load achieved 16.20 MPa, corresponding to in-situ geo-stress conditions representative of a vertical depth of 600 m, excavation and support were performed on the surrounding rock in accordance with the grading control strategy. Subsequently, external load continued to be applied according to the predetermined conditions. The crack propagation in the roadway cross-section and the surrounding rock deformation are presented in Table 3.

Table 3: Deformation and damage characteristics of grade-supported roadway sections

External load / MPa	Cross-section diagram	Deformation characteristics
16.20		The unloaded surrounding rock in the roadway cross-section demonstrated no significant crack development, while the cross-sectional shape remained structurally intact.
19.44		Cracks were observed on the right sidewall of the roadway, while the cross-sectional shape remained essentially unaltered.
22.68		Cracks developed on both sides of the roadway and extended into deeper regions. The shape of the cross-section slightly reduced, and no significant fragment collapse was observed.
25.92		The roadway cross-section shape remained intact, but the number of cracks increased on both sides. Only a few cracks extended along the original ones, and no significant debris falling was observed in the shallow regions.
29.16		Debris began to fall within the roadway, and penetrating cracks appeared at the top. However, these cracks did not significantly extend into deep regions.
32.40		The roadway cross-section narrowed. Cracks in deep regions did not show significant propagation, but existing cracks became more pronounced. The shallow surrounding rock near the roadway surface exhibited damage, and the damaged area was shallow.

Displacements at various measurement points under different stress concentration conditions in the grading control model were recorded, and the results are illustrated in Fig. 8.



(a) 20 cm from the center of the roadway

(b) 25 cm from the center of the roadway

(c) 30 cm from the center of the roadway

(d) 35 cm from the center of the roadway

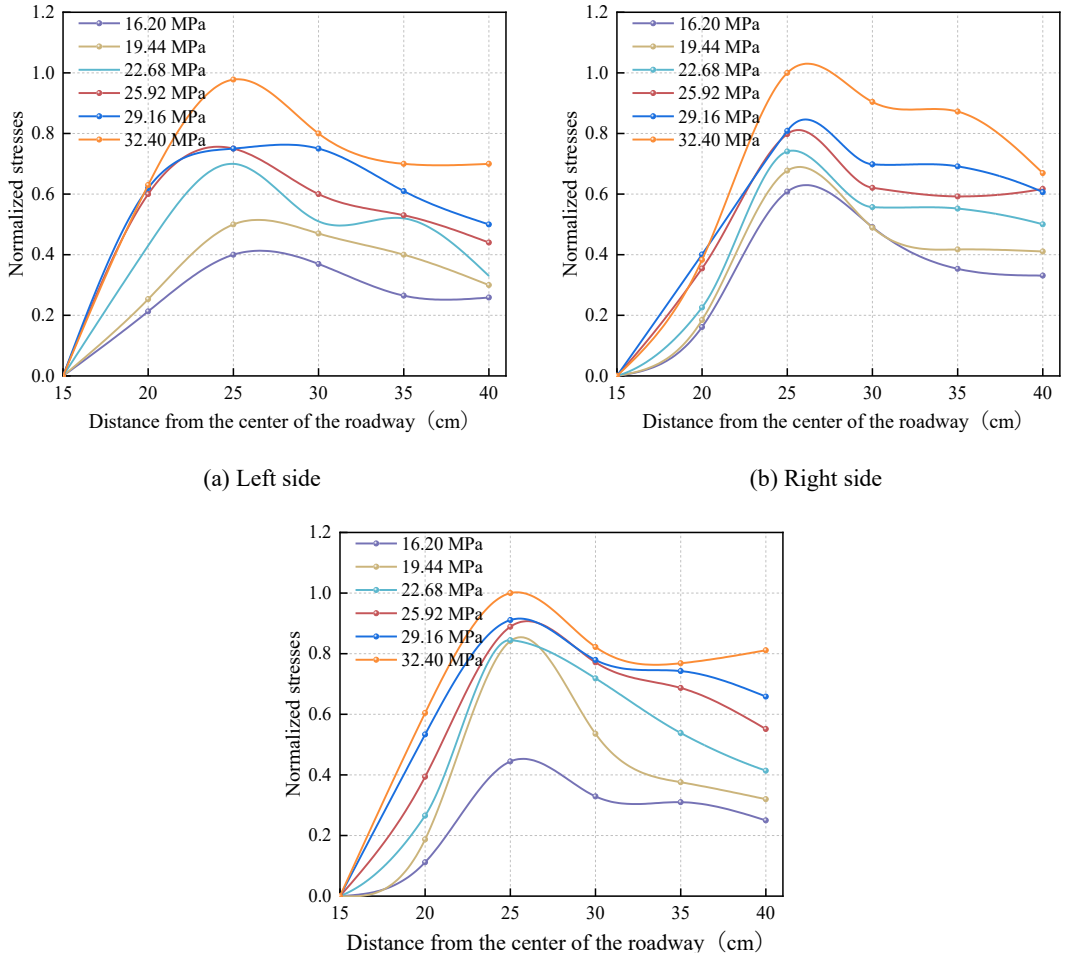
Fig. 8 Macroscopic and detailed results of displacement variations at different depths in graded controlled surrounding rocks

Under grading control conditions, the displacement variations of the surrounding rock at different depths were quite similar. The surrounding rock did not experience collapse or caving. The deformation curves were relatively smooth, with few abrupt changes. With the progressive increase in the externally applied load, the cross-section of the roadway subjected to compressive forces exhibited a progressive reduction in cross-sectional area. When the external load reached 22.68 MPa, the average displacement at 5 cm from the roadway's contour increased by 102.89% compared to 1.1 times the stress concentration scenario, while at 20 cm from the roadway's contour, the average increase was 83.09%. This phenomenon may be attributed to the applied load exceeding the load-bearing capacity of materials within the grouting simulation region, resulting in accelerated deformation rates in the surrounding rock. When the external load reached 29.16 MPa, the average displacement in the shallow surrounding rock at 5 cm from the roadway's contour showed a

298 significant increase of 17.67%. The average displacements at other depths increased by 12.36%,
299 11.89%, and 9.86%, respectively. The deep surrounding rock and support structures in this scenario
300 served as the primary load-bearing elements. As the external load increased to 32.40 MPa, the
301 surrounding rock exhibited varying deformation degrees at different depths, showing the most
302 pronounced deformation in shallow regions.

303 ***5.2.2 Evolution characteristics of the surrounding rock stress***

304 The stress data obtained from pressure sensors were normalized and are presented in Fig. 9.
305 The stress exhibited an initial increase followed by a decrease from the roadway surface progressing
306 into deeper rock strata. The peak stress was located approximately 10 cm from the roadway's contour.
307 The stresses on both sides of the roadway's contour at a distance of 5 m did not exhibit a significant
308 increase when an external load of 25.92 MPa was applied. Furthermore, the stress on the right
309 roadway side exhibited a marginal decrease when an external load of 32.40 MPa was applied. The
310 observed phenomenon can be attributed to progressive damage and failure within the shallow grout
311 zone of the surrounding rock, resulting in diminished load-bearing capacity. Nonetheless, the
312 support system maintained sufficient load-bearing capacity to prevent a stress drop. The surrounding
313 rock at a distance of 10 cm to 25 cm from the roadway's contour did not exhibit any significant
314 cracking and remained intact. The deep stress in this region gradually increased with the rise in
315 external load.



(a) Left side

(b) Right side

(c) Top

Fig. 9 Stress distribution characteristics at different depths

5.2.3 Evolution characteristics of the stresses in support components

The stress characteristic points of anchor rods, anchor cables, and grouted anchor cables under grading control were extracted to analyze the relative variations in the axial forces of these components under different stress concentration conditions, as illustrated in Fig. 10.

The relative stresses obtained from the dynameters installed on the anchor rods, anchor cables, and grouted anchor cables increased with increasing external load. All three normalized stresses of these components at an external load of 16.20 MPa were greater than 0.5. This finding suggested that they provided significant support efficiency. As external load rose to 19.44 MPa, the surrounding rock deformed, while the normalized stresses for all three components increased. This

indicated that their supporting effects on the surrounding rock were strengthened. The order of the stress distribution ratio was anchor rod > anchor cable > grouted anchor cable. As external load increased to a range of 22.68 to 25.92 MPa, the stresses in both anchor rods and anchor cables continued to rise. While the stress in anchor rods exhibited the highest proportion, its rate of increase began to decrease. Under high-stress conditions, the stresses in anchor cables and grouted anchor cables continued to increase. However, the rate of stress increase in anchor cables diminished as the surrounding rock damage intensified. For the surrounding rock under grading control, the increase in the stress in anchor rods was mainly attributed to their substantial support during the low-stress concentration stage. Under stress concentration conditions, there were no noticeable drops in stresses or failures in the support structures of anchor rods, anchor cables, and grouted anchor cables. Even under a scenario of two times the stress concentration, the support structures remained effective and did not reach their load peaks, which confirmed the effectiveness of the grading control strategy.

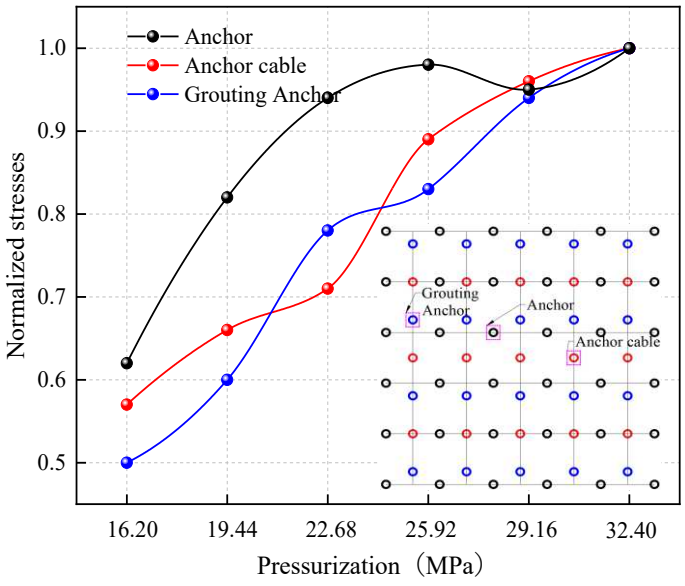


Fig. 10 Trend in relative axial force of anchor rods and anchor cables

In summary, the surrounding rock behind the excavation face was affected by excavation

activities, leading to an increase in stress concentration. In the unsupported scenario, surrounding rock fragmentation extended to approximately 10 m from the roadway's contour, where cracks were well-developed. Consequently, caving and collapse occurred in the unloaded surrounding rock. Under the same conditions, the area of fragmented surrounding rock under grading control was smaller and primarily concentrated within 5 cm from the roadway's contour. In the unsupported scenario, there were more displacement mutation points in the surrounding rock, and large deformation areas were concentrated. Conversely, the displacement curve under grading control was smoother, with more uniform deformation and a wider distribution of deformation range.

The stress distribution under grading control conditions was more uniform than that under unsupported conditions, while no stress drops were observed. The stress exhibited a positive correlation with external loads. The relative axial stress of the anchor rods and anchor cables increased, and the support capacity was enhanced. Even under conditions of twice the original rock stress, the integrity of the surrounding rock was maintained, and the coupled support structure remained stable without significant collapse or instability. This indicates that the PRU strategy of “crack prevention, crack reduction, and pressure relief” effectively maintains the stability.

6 Implementation of grading control for roadway surrounding rock

6.1 Control parameters for field practice

The engineering test was conducted in a section of the 1302 working face haulage roadway in a Shaanxi coal mine. The roadway section in this area is rectangular with clear dimensions of width × height = 5.0 m × 4.0 m, and burial depth ranging from 540 m to 640 m. The immediate roof consists of mudstone with thickness varying between 2.7 m and 7.6 m, while the main roof

comprises fine sandstone and coarse-grained sandstone approximately 23 m thick. The immediate floor primarily features interbedded mudstone and carbonaceous mudstone with a thickness of about 7.1 m, underlain by the main floor composed of fine sandstone and coarse-grained sandstone approximately 17 m thick. According to field monitoring data, the local stress in surrounding rock of the roadway reaches approximately twice the theoretical calculation value.

This study proposes a graded control strategy aimed at ensuring the stability of surrounding rock, comprising three distinct levels: Level I primary support targeting crack prevention, Level II reinforced anchor grouting for crack reduction, and Level III localized drilling implemented for pressure relief. The implementation outcomes are demonstrated in Fig. 11.

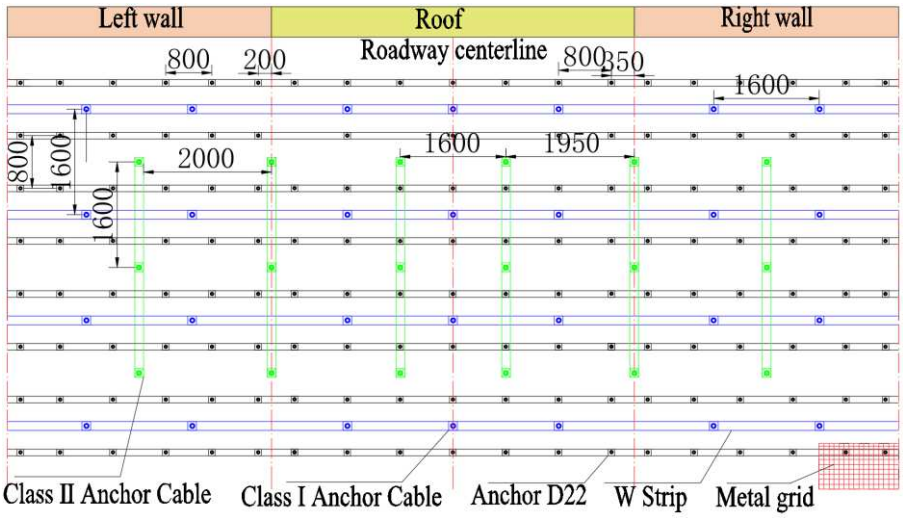


Fig. 11 Stability control support design

6.1.1 Level I stability control

Level I stability control primarily utilizes a combination of anchor rods, anchor cables, steel mesh, and supporting steel strips to establish a primary support system, as illustrated in Fig. 11. The anchor rods are left-handed, high-strength threaded steel bars with dimensions of L×Φ=2400×22 mm, a yield load exceeding 160 kN, and a tensile load greater than 210 kN. They were utilized in conjunction with steel strips and diamond-shaped metal mesh. Each anchor rod was equipped with

one Z2370 resin cartridge and two K2335 resin cartridges. The spacing between rows was set to 800 mm × 800 mm.

The anchor cables utilize steel strands with a diameter of 21.8 mm, configured in a 1×19 structural arrangement. The installed cables in the roof and sidewalls measure 6,200 mm and 4,500 mm in length, respectively. Their tensile strength, elongation, and breaking force are no less than 1,860 MPa, 5%, and 550 kN, respectively. The exposed section of the anchor cable measures 250 mm in length, while the pretension force is maintained at a minimum of 210 kN.

Both the roadway roof and sidewalls employ diamond-shaped metal woven mesh. The specifications for the metal mesh at the roof and sidewalls are L×B = 6,000×1,000 mm and L×B = 4,000×1,000 mm, respectively. The mesh grid dimensions are L×B = 50×50 mm. The W steel strips are made from the 5 mm thick steel plate. The components have a width of 180 mm and a length of 3500 mm, with hole spacing set at 1600 mm. Roof flat steel strips measure 180 mm in width, 5000 mm in length, and 5 mm in thickness, while sidewall strips are 150 mm wide, 3400 mm long, and 3 mm thick, with both configurations maintaining an 800 mm hole spacing.

6.1.2 Level II stability control

Level II control aims to ensure the long-term stability of coal roadways by expanding the scope of grouting and support. After implementing Level I control, longer anchor cables with a diameter of 21.6 mm were installed in a 1×7 configuration. The lengths of the anchor cables installed at the roof and sidewalls are 8,600 mm and 4,500 mm, respectively. Their tensile strength, elongation, and breaking force are no less than 1860 MPa, 5%, and 550 kN, respectively. The anchor cable washers use steel disc-shaped washers, with flat specifications of not less than 300 mm × 300 mm × 15 mm. The exposed length of the anchor cables is between 150 mm and 250 mm. The anchor cables were

used in conjunction with W steel strips. Each anchor cable is equipped with two Z2370 resin cartridges and one K2335 resin cartridge. The spacing between rows was set to 1,600 mm×1,600 mm. The prestress is not less than 210 kN.

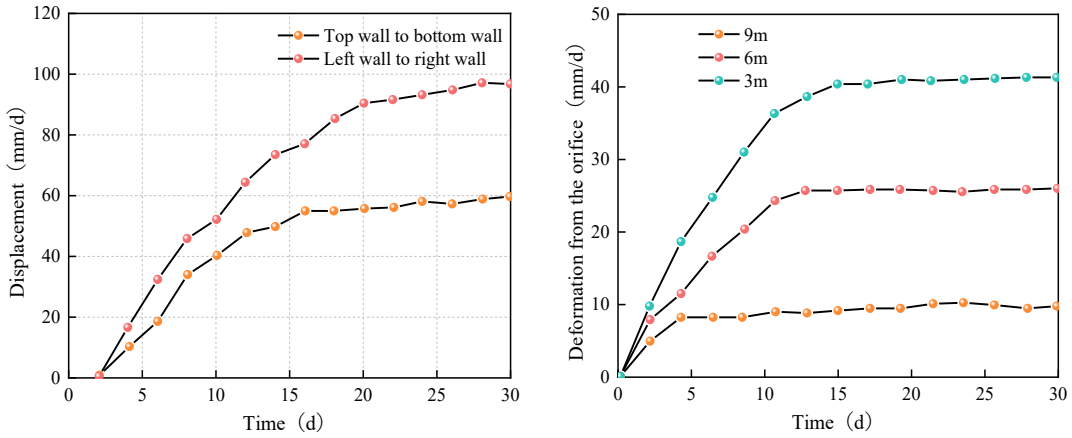
A self-developed integrated anchoring-grouting device and custom grouting materials for surrounding rock reinforcement were utilized during the installation of anchor cables for secondary reinforcement (Huang et al. 2022). The water-to-cement ratio was controlled within 0.6-0.75, with the grouting pressure regulated to 2.5-3.5 MPa.

6.1.3 Level III stability control

Level III control focuses on ensuring long-term stability of coal roadway by selecting appropriate times for drilling and pressure relief based on the mining pressure patterns. The borehole was designed with a diameter of 153 mm, an opening distance from the floor of 1.4 to 2.0 m, an inclination angle of 5°, and a depth of 20 m. The average spacing between the boreholes was set at 2.5 m.

6.2 Analysis of grading control effectiveness

A ground pressure monitoring station was established in the trial area of the 1302 working face machine roadway. Laser rangefinders and multi-point displacement meters were deployed to respectively monitor surface deformation of surrounding rock and borehole displacement, aiming to evaluate the effectiveness of graded support systems for deteriorated surrounding rock in high-stress roadways.

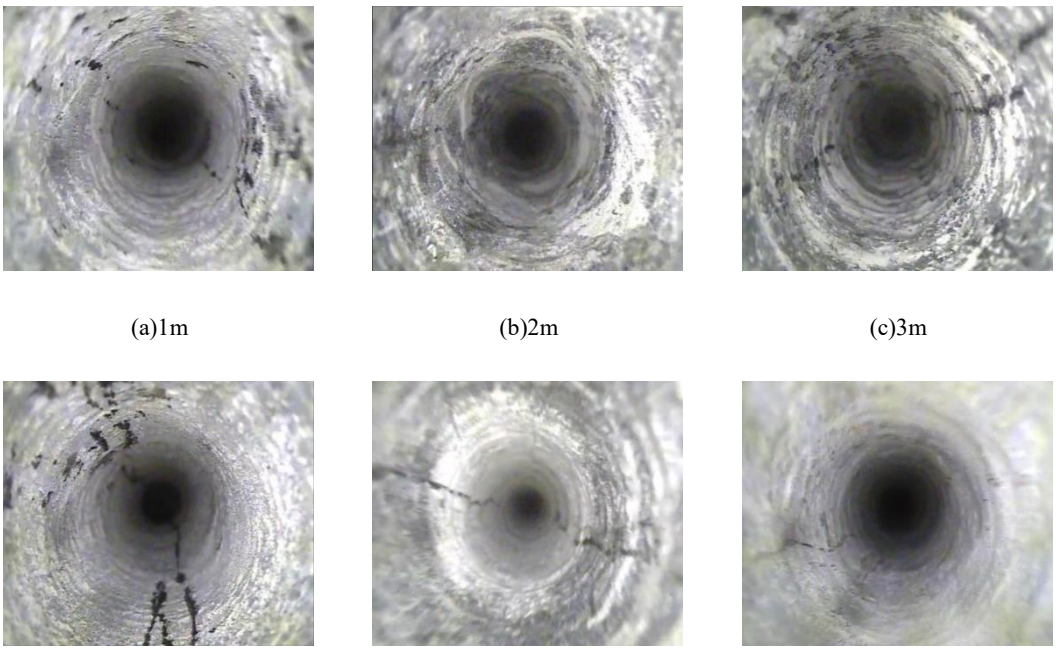


(a) Surface displacement monitoring

(b) Top wall delamination monitoring

Fig. 12 Deformation monitoring of the surrounding rock

The observations of the roof delamination are depicted in Fig. 12(b). The analysis revealed that following the implementation of graded control measures, the deformation rate of the surrounding rock exhibited a gradual decrease followed by stabilization. The displacements at the deep reference points relative to the borehole opening were greater than those at the shallow reference points. The differences in displacement among the reference points were minimal, indicating an overall favorable control effect. This suggested that there were no significant separations between the deformed surrounding rock layers. The synergistic application of structural support and grouting techniques that penetrated micro-fractures within the surrounding rock significantly improved the load-bearing capacity. The deep-seated surrounding rock maintained deformation characteristics within acceptable geomechanical parameters. These findings provide empirical validation that the graded control methodology effectively maintains the structural integrity and operational safety of the roadway.

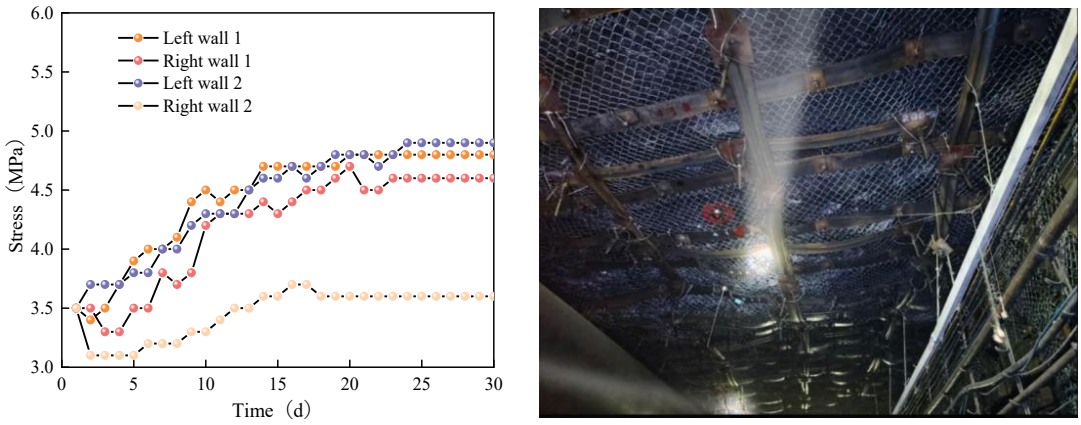


(a)1m (b)2m (c)3m

(d)4m (e)5m (f)6m

Fig. 13 Test results for drilling peepholes

A borehole camera was utilized in the roadway test section to inspect the measurement holes. The findings are presented in Fig. 13, which illustrates the fracture development within the boreholes. The inspection results revealed that after the integrated anchor cable-grouting operations, the borehole walls were relatively smooth. The distribution of the grouting material was clearly observable but decreased gradually with increasing borehole depth. The smooth walls of the drill boreholes indicated that the surrounding rock in this section remained intact, with no major delamination occurring after the implementation of grading support control.



(a) Borehole stress gauge monitoring (b) On-site support effect

Fig. 14 Stress monitoring and actual map of the site

Boreholes of 10m depth were drilled on both sides of the roadway, with borehole stress meters installed at the bottom of the holes. The monitoring results are shown in Fig. 14. The stresses in the boreholes initially increased and then stabilized. The stable surrounding rock stress demonstrated that after the implementation of grading control, there was no noticeable stress concentration. The stress environment was found to be favorable. The surrounding rock deformation exhibited a marked reduction, while the cross-sectional geometry was preserved within acceptable tolerance thresholds. These results demonstrate that the graded control technique effectively mitigates substantial deformation phenomena in excavated roadways while maintaining structural stability of the mechanically unloaded surrounding rock mass.

7 Conclusions

(1) This study proposes an integrated control approach designed to prevent crack initiation, minimize crack propagation, and mitigate stress concentration. A grading control strategy was established, which includes Level I: primary support for crack prevention, Level II: reinforced anchor grouting for crack reduction, and Level III: localized drilling for pressure relief.

(2) Physical model experiment proved taht under unsupported conditions, as external load rose,

cracks in the surrounding rock extended from shallow to deeper regions. The surrounding rock experienced substantial fragmentation. Stress magnitudes decreased in shallow regions while increasing in deeper zones, with the peak stress migrating toward deeper strata.

(3) Physical model experiment proved taht under grading control conditions, the surrounding rock in the high-stress roadway exhibited minimal damage. Under stress concentration conditions, the stresses in the anchor rods, anchor cables, and grouted anchor cables increased with rising external load, and no support failures were observed. Grading control strategy effectively contributes to the stability of the unloaded surrounding rock.

(4) Field applications demonstrated minimal roadway deformation, favorable grouting performance, and an improved surrounding rock stress state. Grading control strategy effectively ensures the stability of the unloaded surrounding rock.

Author contributions Methodology, formal analysis, writing—original draft preparation, and writing—review and editing: Chongyan Liu, Cheng Pan, Guangming Zhao, and Longpei Ma. Similarity simulation experiment: Chongyan Liu, Qihang Zhang, and Cheng Pan. Supervision and project administration: Longpei Ma and Guangming Zhao. All authors have read and agreed to the published version of the manuscript.

Funding This work was supported by the Key Laboratory of Safe and Effective Coal Mining (Anhui University of Science and Technology) Ministry of Education (JYBSYS202504), the Anhui University of Science and Technology Talent Recruitment Fund (2025yjrc0107), the National Natural Science Foundation of China (U25A20270), the National Natural Science Foundation of

China (52374074, 52404068, 52604101).

Availability of data and materials The data that support the findings of this work are available from the corresponding author.

Declarations

Ethical approval and consent to participate Not applicable.

Consent to publication All authors approved the final manuscript and the submission to this journal.

Competing interests The authors declare no competing interests.

Open Access This article is licensed under a Creative Commons Attribution-NonCommercial-NoDerivatives 4.0 International License, which permits any non-commercial use, sharing, distribution and reproduction in any medium or format, as long as you give appropriate credit to the original author(s) and the source, provide a link to the Creative Commons licence, and indicate if you modified the licensed material. You do not have permission under this licence to share adapted material derived from this article or parts of it. The images or other third party material in this article are included in the article's Creative Commons licence, unless indicated otherwise in a credit line to the material. If material is not included in the article's Creative Commons licence and your intended use is not permitted by statutory regulation or exceeds the permitted use, you will need to obtain permission directly from the copyright holder. To view a copy of this licence, visit http://creativecommons.org/licenses/by-nc-nd/4.0/.

References

Bednarek L, Małkowski P, Niedbalski Z, Mucha K (2024) Steel arch and rock bolt support in terms of the Gateroad stability maintaining behind the longwall face. Appl Sci 14(9):3594. https://doi.org/10.3390/app14093594

Cai MF, Brown ET (2017) Challenges in the mining and utilization of deep mineral resources. Engineering 3(4):432-433. https://doi.org/10.1016/J.ENG.2017.04.027

Chen DC, Ji CW, Xie SR, Wang E, He FL, Cheng Q, Zhang Q (2020) Deviatoric stress evolution laws and control in surrounding rock of soft coal and soft roof roadway under intense mining conditions. Adv Mater Sci Eng 2020(1):5036092. https://doi.org/10.1155/2020/5036092

Dong CL, Zhao GM, Lu XY, Meng XR, Li YM, Cheng X (2018) Similar simulation device for unloading effect of deep roadway excavation and its application. J Mt Sci 15(5):1115-1128. https://doi.org/10.1007/s11629-017-4784-2

Huang SJ, Zhao GM, Meng XR, Cheng X, Gu QH, Liu G, Zhu SK (2022) Development of cement-based grouting material for reinforcing narrow coal pillars and engineering applications. Processes 10(11):2292. https://doi.org/10.3390/pr10112292

Kang HP, Gao FQ, Xu G, Ren HW (2023) Mechanical behaviors of coal measures and ground control technologies for China's deep coal mines–A review. J Rock Mech Geotech Eng 15(1):37-65. https://doi.org/10.1016/j.jrmge.2022.11.004

Kang HP, Li JZ, Yang JG, Gao FQ (2017) Investigation on the influence of abutment pressure on the stability of rock bolt reinforced roof strata through physical and numerical modeling. Rock Mech Rock Eng 50(2):387-401. https://doi.org/10.1007/s00603-016-1114-x

Li SC, Wang HT, Wang Q, Jiang B, Wang FQ, Guo NB, Liu WJ, Ren YX (2016) Failure mechanism of bolting support and high-strength bolt-grouting technology for deep and soft surrounding rock with high stress. J Cent South Univ 23(2):440-448. https://doi.org/10.1007/s11771-016-3089-x

Li ZD, Song JH, Wu BY, Zha ES, Li P, Xu D, Li JF, Fang J, Yu ML (2025) Multifield Coupling Evolution Characteristics and Water Storage Stability Analysis of Steep Coal

Seam Roadway Based on Similar Physical Simulation Tests. Int J Energy Res 2025(1): 4554562. https://doi.org/10.1155/er/4554562

Liu CY, Pan C, Zhao GM, Xu WS, Meng XR, Liu WJ, Cheng X (2025b) Experimental study on the failure mechanism of roadway surrounding rock under true triaxial loading: Insights from acoustic emission (AE) characteristics. Measurement 246:116727. https://doi.org/10.1016/j.measurement.2025.116727

Liu CY, Zhao GM, Pan C, Meng XR, Xu WS, Liu WJ (2025a) Damage analysis and grading control technology of surrounding rock in high geo-stress roadway. Sci Rep 15 (1):1188. https://doi.org/10.1038/s41598-025-85647-2

Liu RT, Zhou Z, Li SC, Zhang QS (2019) Study on grouting penetration in soil rock mixture and the mechanical behavior after grouting reinforcement. J Test Eval 47(3):2240-2254. https://doi.org/10.1520/JTE20170761

Małkowski P, Ostrowski L (2019) Convergence monitoring as a basis for numerical analysis of changes of rock-mass quality and Hoek-Brown failure criterion parameters due to longwall excavation. Arch Min Sci 64(1):93-118. https://doi.org/10.24425/ams.2019.126274

Nan H (2012) Similar simulation research on top coal's failure process. J Comput Theor Nanosci 9(9):1205-1208. https://doi/10.1166/jctn.2012.2171

Peng K, Yi GS, Luo S, Si XF (2023) Stress analysis and spalling failure simulation on surrounding rock of deep arch tunnel. Appl Sci 13(11):6474. https://doi.org/10.3390/app13116474

Qiu JD, Huang R, Wang HW, Wang F, Zhou CT (2025) Rate-dependent tensile behaviors of jointed rock masses considering geological conditions using a combined BPM-DFN model: Strength, fragmentation and failure modes. Soil Dyn Earthq Eng 195:109393. https://doi.org/10.1016/j.soildyn.2025.109393

Romashov AN, Tsygankov SS (1993) Generalized model of rock bursts. J Min Sci 28(5):420-423. https://doi.org/10.1007/BF00711122

Si X, Luo Y, Luo S (2024) Influence of lithology and bedding orientation on failure behavior of “D” shaped tunnel. Theor Appl Fract Mech 129:104219. https://doi.org/10.1016/j.tafmec.2023.104219

562 Sun FW, Sun ZY, Zhang DL, Li MY (2024) Large-scale model test and numerical analysi
563 s of load-bearing arch characteristics of large cross-section tunnel under high geostres
564 s. Eng Fail Anal 163:108600. https://doi.org/10.1016/j.engfailanal.2024.108600
565 Vacek J, Chocholoušová J (2008) Rock burst mechanics: insight from physical and mathe
566 matical modelling. Acta Polytech 48(6). https://doi.org/10.14311/1071
567 Wang P, Zhang N, Kan JG, Wei Q, Xie ZZ, Li A, He Z, Qi JH, Xu XL, Duan CR (202
568 4) Accumulated damage failure mechanism of anchoring structures under cyclic impact
569 disturbance. Int J Min Sci Technol 34(12):1693-1709. https://doi.org/10.1016/j.ijmst.20
570 24.11.006
571 Wang Q, Qin Q, Jiang B, Yu HC, Pan R, Li SC (2019) Study and engineering applicatio
572 n on the bolt-grouting reinforcement effect in underground engineering with fractured
573 surrounding rock. Tunn Undergr Space Technol 84:237-247. https://doi.org/10.1016/j.tus
574 t.2018.11.028
575 Wu M, Ye YC, Wang QH, Hu NY (2022) Development of rockburst research: a comprehe
576 nsive review. Appl Sci 12(3):974. https://doi.org/10.3390/app12030974
577 Xiang Z, Zhang N, Qian DY, Xie ZZ, Zhang CH, Guo F, Wang S (2021) Failure charact
578 eristics and stability control of bolt support in thick-coal-seam roadway of three typic
579 al coal mines in China. Shock Vib 2021(1):5589085. https://doi.org/10.1155/2021/55890
580 85
581 Xie SR, Li H, Chen DF, Feng SH, Ma X, Jiang ZS, Cui JQ (2022) New technology of
582 pressure relief control in soft coal roadways with deep, violent mining and large defo
583 rmation: A key study. Energies 15(23):9208. https://doi.org/10.3390/en15239208
584 Xie ZZ, Li YL, Zhang N, He Z, Cao C, Li W (2023) Model experiment research on HP
585 TL anchoring technology for coal-rock composite roof in deep roadway. Sci Rep 13
586 (1):2381. https://doi.org/10.1038/s41598-023-29232-5
587 Yang SQ, Chen M, Jing HW, Chen KF, Meng B (2017) A case study on large deformatio
588 n failure mechanism of deep soft rock roadway in Xin'An coal mine, China. Eng Ge
589 ol 217:89-101. https://doi.org/10.1016/j.enggeo.2016.12.012
590 Yang ZQ, Liu C, Dong Y, Dou LM, Wu JK (2019) Study on properties of grouting mater
591 ials and reinforcement effect in coal roadways influenced by dynamic pressure. Geotec

592 h Geol Eng 37(4):3329-3342. https://doi.org/10.1007/s10706-019-00847-8
593 Zhang ZR, Wu SC, Cheng HY, Han LQ, Zhong G, Zhang J (2024) Rockburst simulation
594 tests on structural plane of deep high-stress circular tunnels: A true triaxial test study
595 on several different hard rocks. Theor Appl Fract Mech 132:104473. https://doi.org/10.
596 1016/j.tafmec.2024.104473
597 Zhao CX, Li YM, Liu G, Chen DG, Meng XR (2020) Research on the stress distribution
598 law of fully anchored bolt and analysis of influencing factors under the condition of
599 surrounding rock deformation. Adv Civ Eng 2020(1):8818375. https://doi.org/10.1155/2
600 020/8818375
601 Zhu GQ, Li S, Li C, Liu G, Zhou YY (2023) Physical model study on brittle failure of
602 pressurized deep tunnel with support system. Rock Mech Rock Eng 56(12):9013-9033.
603 https://doi.org/10.1007/s00603-023-03541-7
604 Zhuang JX, Mu ZL, Zhang XF, Cai W, Cao AY, Jiang CL, Małkowski P (2023) Seismic
605 mitigation effect of overlying weakening strata in underground coal mines. Energies 1
606 6(16):5958. https://doi.org/10.3390/en16165958
607

Supplementary Files

This is a list of supplementary files associated with this preprint. Click to download.

- Articlehighlights.docx
- Declarations.docx
- CoverLetter.docx